Editors' Suggestion | Featured in Physics

Synchronization of Bloch Oscillations in a Strongly Coupled Pair of Small Josephson Junctions: Evidence for a Shapiro-like Current Step

Fabian Kaap,[1] David Scheer,[2] Fabian Hassler,[2] and Sergey Lotkhov[1,*]
[1]Physikalisch-Technische Bundesanstalt, Bundesallee 100, 38116 Braunschweig, Germany
[2]JARA Institute for Quantum Information, RWTH Aachen University, 52056 Aachen, Germany

(Received 12 June 2023; revised 1 September 2023; accepted 15 November 2023; published 12 January 2024)

Bloch oscillations are a fundamental phenomenon linking the adiabatic transport of Cooper pairs to time. Here, we investigate synchronization of the Bloch oscillations in a strongly coupled system of sub-100 nm $Al/AlO_x/Al$ Josephson junctions in a high-Ohmic environment composed of highly inductive meanders of granulated aluminum and high-Ohmic titanium microstrips. We observe a pronounced current mirror effect in the coupled junctions and demonstrate current plateaus, akin to the first dual Shapiro step in microwave experiments. These findings suggest that our circuit design holds promise for realizing protected Bloch oscillations and precise Shapiro steps of interest for current metrology.

DOI: 10.1103/PhysRevLett.132.027001

In the last decade, the international system of units has undergone a major change by fixing the value of fundamental constants [1]. On the one hand, the ac-Josephson effect is widely used to connect the voltage to frequency via the so-called Shapiro voltage steps leading to a quantum voltage standard [2]. On the other hand, the realization of the ampere has been only indirectly referred to frequency, by linking the Josephson-voltage and quantum-Hall resistance standards. Referring the current directly to frequency, thus closing the metrology triangle, is the important next step in the reorganization of the unit system. It would allow one to make current measurements more accurate, test the consistency of the unit system, and detect changes in the value of the fundamental constants over time.

The straightforward idea to define current by counting the elementary charges e that pass per unit time is realized in quantum pumps [3]. However, they turn out to be difficult to realize for current values above $\sim$1 nA of practical interest. An alternative idea is to use Bloch oscillations in Josephson junctions with a small capacitance in order to arrange a quantum coherent transport of single Cooper pairs with charge $2e$. Subjecting the junction to a constant bias current I_B, its capacitance charges up until $2e$ is loaded, at which points the transport of a Cooper pair discharges the capacitance. This charging and discharging sequence leads to an oscillating voltage at frequency $f_B = I_B/2e$, the so-called Bloch oscillations [4].

In a number of experiments (see, e.g., Refs. [5–7]), Bloch oscillations were synchronized to an external drive at fixed frequency. This gives rise to dual Shapiro steps of quantized current predicted by theory [4,8]. The early Bloch oscillation circuits necessarily included high-Ohmic biasing resistors, implemented in order to reduce the quantum fluctuations of charge and to suppress inelastic tunnel processes. In experiments, this resulted in strong electron overheating, the dramatic increase of thermal fluctuations, and, finally, in washing out the coherent oscillation effects [5,9,10].

As a remedy, a combined, resistive, and inductive environment was theoretically proposed as a viable alternative to the purely resistive one [11]. This alternative approach has recently been implemented using either high-kinetic inductance elements made of thin NbN films in Ref. [6] or Josephson inductances in a long array of Josephson junctions [7]. However, as shown in Ref. [6], inelastic tunneling processes that come into play due to finite effective temperature, $T_{\mathrm{eff}} \sim 100$ mK, and high, but limited bias impedance, still impose severe restrictions on the flatness of the resulting current steps.

Considerable improvement could be achieved using the dipole charge transfer in a symmetric, strongly coupled pair of Bloch junctions, see Fig. 1, with different charging energy scales for coherent $\sim e^2/2C_c$ and inelastic

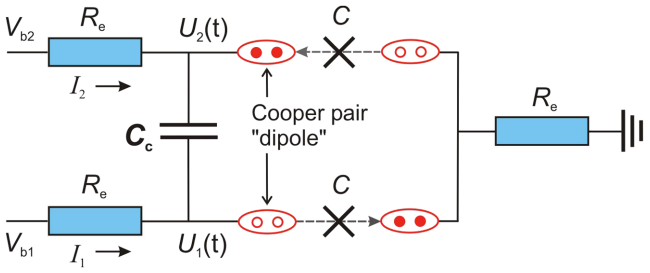

FIG. 1. A symmetric circuit with two coupled Josephson junctions allowing for the synchronization of Bloch oscillations. The signature of this is the current mirror effect with $I_1 = -I_2$, appearing due to transport via Cooper pair dipoles indicated in red, see main text for details. Note that, in order to achieve coherent Bloch oscillations, the bias resistances must exceed the resistance quantum with $R_e \gg R_Q = h/4e^2 \approx 6.45$ kΩ.

$\sim e^2/2C \equiv E_C$ Cooper pair processes, where $C_c \gg C$ are the coupling and the tunnel capacitances, respectively. In such a circuit, the competing single Cooper pair processes are expected to be subdominant compared to the coherent dipole transfers keeping the voltage across the junctions small, $U_{1,2} \sim (e/C_c)/2 \ll e/C$. A related setup has been proposed in Ref. [12] for constructing a protected qubit based on dipole transport (dubbed "current mirror") in a Josephson ladder. Experimentally, the current mirror effect with the signal correlation of up to 98.8% was demonstrated by studying the switching voltage statistics in two superconducting 1D arrays [13].

In this Letter, we present the results of our dc characterization for a strongly coupled pair of Bloch oscillators enabling the dipole transport discussed above. We study an asymmetric circuit shown in Fig. 2, with a small superconducting quantum interference device (SQUID) in one current arm as a Bloch oscillator with a tunable amplitude. The junctions were coupled capacitively using two in-line meanders in series to high-Ohmic resistive leads. We show the tunable-capacitor behavior, observed at zero bias current in SQUID and also, more importantly, the current mirror effect in the two-currents plane resulting from the synchronization of the two Bloch oscillations in the sub-GHz range. Because of the synchronization of the Bloch oscillations that antialigns the dc currents in both arms, the data exhibit a pronounced current step with a step value that is akin to the first dual Shapiro step induced by an external GHz signal [5–7]. The data are consistent with a theory providing an interpretation in terms of correlated adiabatic ground state transport.

The experimental circuit was fabricated using e-beam-exposed PMMA/copolymer liftoff masks with a controllable undercut [14] and the shadow evaporation technique [15]. The Josephson junctions of type $\mathrm{Al/AlO_x/Al}$ were deposited in the common three-angle evaporation process [16] with the coupling meanders made of granulated aluminum (grAl), see, e.g., Ref. [17]. The first Al layer was oxidized at $P_{O2} = 0.3$ Pa for 5 min to enable small junctions, see Fig. 2(c), of low normal resistance $R_N \approx 6$ kΩ and high values of the Josephson energy $E_J = h\Delta/8e^2R_N \approx 110$ μeV and $E_C \approx 150$ μeV, estimated roughly for a single junction and for the superconducting gap value of aluminum $\Delta \approx 200$ μeV, using cofabricated test devices [16]. We note that a similar device with slightly different parameters exhibited widely identical behavior as reported below.

For high-impedance biasing, the meander geometry was preferred, in order to minimize the stray lead capacitance [18]. The kinetic inductance of grAl was estimated within the BCS approximation [19], to achieve $L_{\mathrm{kin},\square} = 0.18\hbar R_n/k_B T_c \approx 0.5$ nH, for the measured values of the grAl normal state resistance $R_{n,\square} \approx 700$ Ω and $T_c \approx 1.9$ K. As a result, the resonance frequency of the TEM wave along the meanders, $\omega_p = (2L_{\mathrm{kin}}C_c)^{-1/2} \sim 2\pi \times 1.3$ GHz, ranged over the frequencies in our experiment. At lower

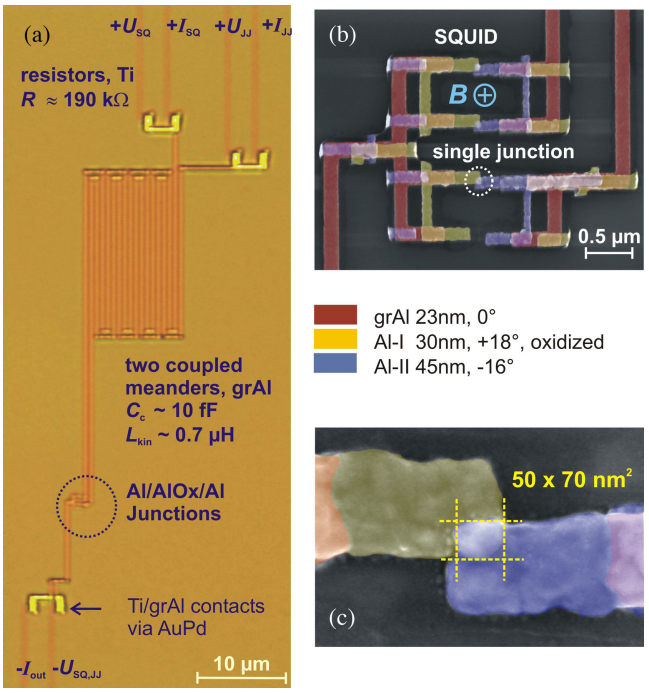

FIG. 2. (a) Optical picture of high-impedance circuitry. Both current arms include titanium microstrips, $20 \times 0.16 \times 0.15$ μm³ long/wide/thick each, as well as 0.14 μm wide meandered lines of grAl. (b) False-colored SEM image of the SQUID and single junction structure. Comparing to Fig. 1, the junction (SQUID) plays the role of the first (second) current arm. (c) Close-up view of a single junction marked by the dashed circle in (b).

frequencies, the condition $R_e \gg R_Q$ was ensured by high-Ohmic titanium microstrips coevaporated with oxygen [20] at $P_{O2} = 3 \times 10^{-4}$ Pa and featured by high film resistivity, $r \approx 1.5$ kΩ per square sheet.

The sample was measured in a filtered environment at $T \approx 15$ mK. The dc currents were supplied symmetrically through pairs of room temperature resistors, $R_b = 2 \times 100$ MΩ, reaching the sample via $\ell \approx 1$ m long Thermocoax filters of capacitance $c\ell \sim 0.5$ nF each [21], mounted in direct vicinity of the chip. At microwave frequencies, such an environment realizes the condition of voltage biasing adopted in Fig. 1.

The diagram in Fig. 3(a) maps the voltage U_{JJ} across the junction vs bias current I_{JJ} at zero current biasing of the SQUID. The magnetic field B and therefore the loop frustration, $f \equiv \Phi_{ext}/\Phi_0$, are varied over a few modulation cycles. Here $\Phi_{ext} = BA$ is the flux threading the loop area $A \approx 0.4$ μm² [see SEM image in Fig. 2(b)] and $\Phi_0 = h/2e$ is the magnetic flux quantum. In this small signal regime, illustrated in Figs. 3(b) and 3(c), the SQUID plays the role of a tunable Bloch capacitance $C_B(U_2, f) \approx C_B(0, f)$ (see, e.g., Ref. [22]), in series to the intermeander capacitance C_c and both in parallel to the single junction [23]. At weak frustration $f \approx 0 \bmod 1$ ($B = 23.1$ mT), with a strong Josephson coupling in the SQUID, the junction turns out

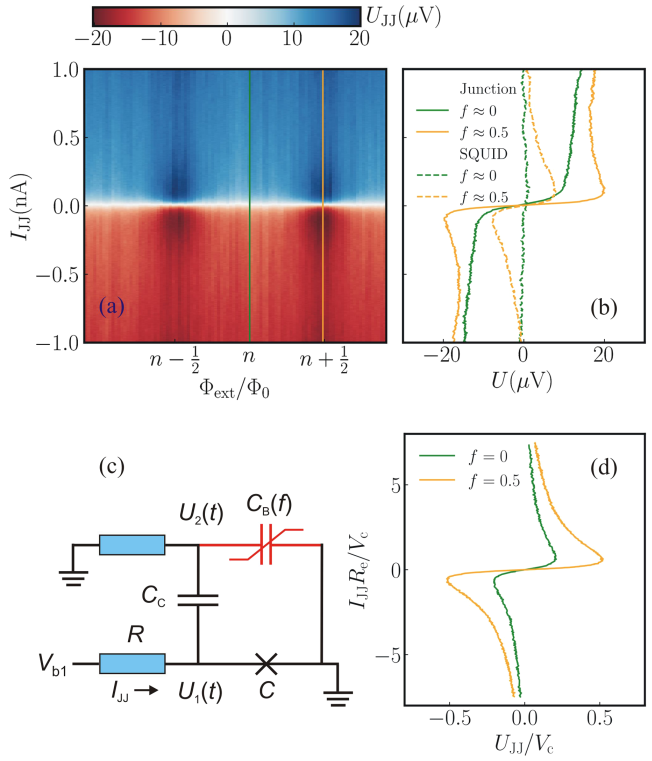

FIG. 3. (a) dc junction voltage $U_{JJ} = \overline{U_1(t)}$ measured as a function of current I_{JJ} and magnetic flux Φ_{ext} at $I_{SQ} = 0$. The green (orange) vertical line marks weak (strong) magnetic frustration of the SQUID, for which the cross-sectional I-V curves are plotted in (b). The dashed lines in (b) depict the dc voltage $U_{SQ} = \overline{U_2(t)}$ induced across the SQUID. (c) Equivalent circuit as a single junction shunted via the Bloch capacitance realized by the SQUID. (d) Simulation of the I-V curves. The values of the parameters are those of Figs. 4(c) and 4(d).

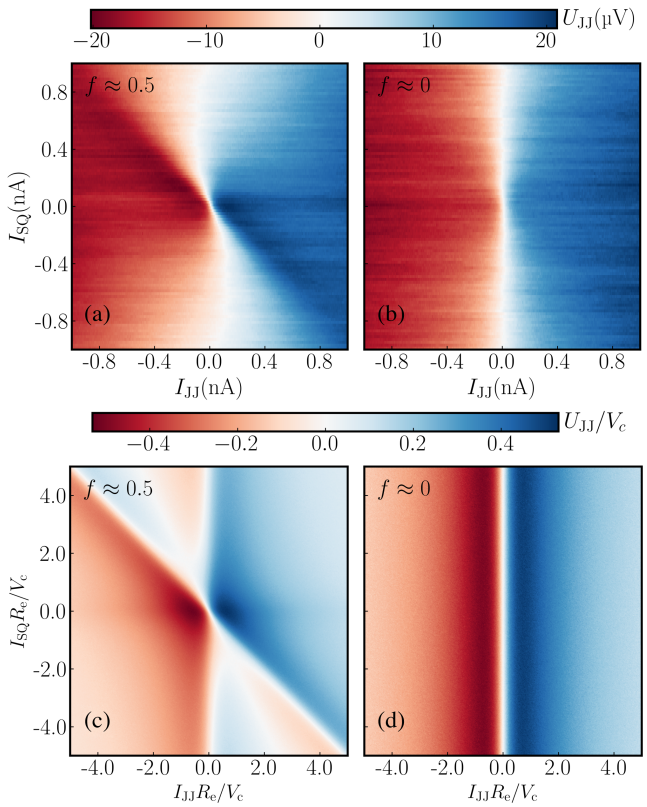

FIG. 4. (a),(b) Voltage U_{JJ} as a function of the two bias currents for the two frustration cases. (c),(d) The simulated data with Johnson-Nyquist noise at a constant temperature of $k_B T = 0.25 e V_{c1}$ in the regime of (c) symmetric Josephson energies and Bloch critical voltages $V_c \equiv V_{c1} = V_{c2} = V_+$ and (d) the single junction regime $V_{c2} = V_+ = 0$.

to be effectively shunted by a larger capacitance C_c: $C \ll C_c \ll C_B(0,0)$. This leads to a small Coulomb blockade threshold, see Figs. 3(b) and 3(d). On the contrary, at strong frustration $f \approx 0.5$ mod 1 ($B = 25.9$ mT), the Bloch and therefore the total shunting capacitance are reduced, resulting in a stronger Coulomb blockade effect. The I-V curve shows a clear backbending, a "fingerprint" of Bloch oscillations.

In the two-current plane (I_{JJ}, I_{SQ}), shown in Fig. 4, the voltage landscape also depends on the magnetic frustration in the SQUID. The diagram in Fig. 4(a), measured close to a half-integer value of f, is asymmetric and shows a singularity of the profile along the line $I_{JJ} = -I_{SQ}$, demonstrating the current mirror effect in the circuit. Qualitatively, the same voltage profile has been observed for the SQUID voltage U_{SQ} as well (not shown). In this regime, the Bloch oscillations in both arms are of appreciable amplitude. They are coupled to each other via the capacitance C_c, giving rise to the plateaus with slow current ramping $I_{JJ}(U_{JJ})$, shown in Fig. 5(a). The ramping of the plateaus, weak at small currents $I_{SQ} \sim 0.1$ nA, is increased toward higher drive currents, in a good agreement with the simulated dynamics, the results shown in Fig. 5(b). Our numerical analysis described in detail below shows that the plateaus are due to synchronization, akin to the first dual Shapiro step reported for the microwave drive signals in Refs. [5–7].

On the contrary, at weak frustration and strong SQUID coupling, we measure a smooth and symmetric disappearance of the blockade feature, as the absolute value of current I_{SQ} is increasing, see Fig. 4(b). This behavior, typical for growing thermal fluctuation effects, is caused by electron overheating in the titanium resistors [24]. The current mirror effect due to the synchronization is missing [cf. Fig. 4(d)] as the amplitude of the Bloch oscillations in SQUID is small [cf., e.g., Fig. 3(b)].

We compare the experimental data with the results of simulations based on Kirchhoff's equations,

$$V_{bi} = R_e(\dot{Q}_i + \dot{Q}_+) + V_{ci} \sin\left(\frac{\pi Q_i}{e}\right) + V_+ \sin\left(\frac{\pi Q_+}{e}\right),$$

for the charges Q_i supplied by the individual leads with a combined charge $Q_+ = Q_1 + Q_2$. In addition to the bias

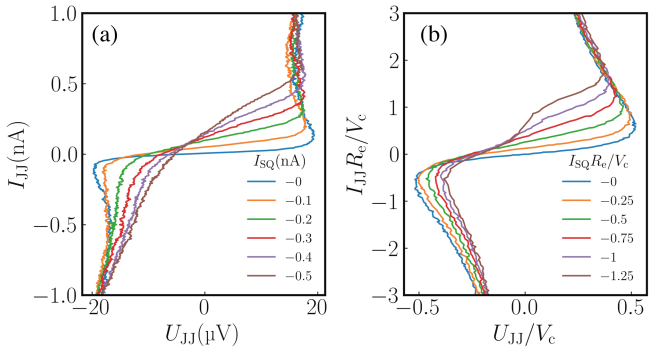

FIG. 5. (a) Current in the junction plotted vs junction voltage at $f \approx 0.5$ and I_{SQ} varying from 0 to 0.5 nA (bottom to top). (b) Simulated data for the synchronized Bloch oscillations in the regime of symmetric Josephson energies for an equidistant series of SQUID current values I_{SQ}.

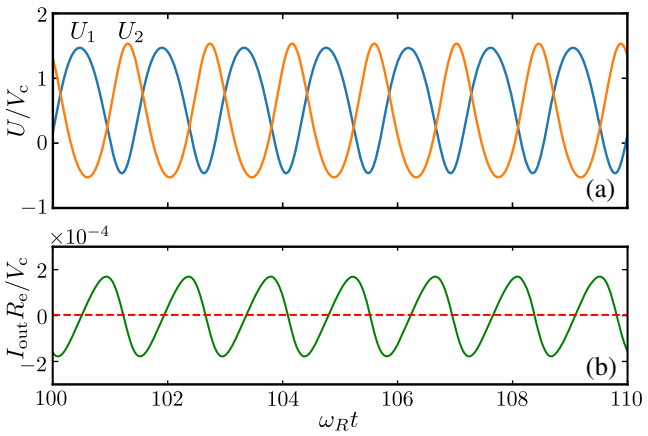

FIG. 6. Simulation of the time-resolved synchronization of Cooper pair transfers in the regime of symmetric Josephson energies with asymmetric bias voltages $V_{b1} = 5V_{c1}$, $V_{b2} = -4V_{c1}$. (a) Voltage drop U_1 (U_2) across the junction (SQUID). (b) A small common node current I_{out} through the lower biasing resistor indicates a current mirror effect.

voltages V_{bi} and the voltage drops over the resistors R_e (first term), the equations contain the voltage drops U_i across the junctions (remaining terms), see the Supplemental Material [25] for the derivation. It consists of the voltage due to individual phase slips with a critical voltage V_{ci} and the term with critical voltage V_+ describing coupled phase slips due to C_c. It is this last term that synchronizes the Bloch oscillations and leads to the current plateaus.

We integrate the equations of motion using the forward Euler method to obtain the voltage drop $U_1(t)$ across the junction for different junction currents. In order to resolve the dynamics at the characteristic frequency of the junction's Bloch oscillations $\omega_R = \pi V_{c1}/eR_e$, we choose discrete time steps of the duration $\delta = 0.25/\omega_R$. We include the effects of Johnson-Nyquist noise from the biasing resistors as Gaussian white noise increments with standard deviation $2R_e k_B T/\delta^{1/2}$. For simplicity and deviating from the experimental conditions with growing thermal smearing effects at increasing currents I_{JJ} and I_{SQ}, the simulations were performed at a constant temperature $k_B T = 0.25eV_{c1}$, which corresponds to $T \approx 150$ mK at $V_{c1} \approx 50$ μV.

We obtained simulation results for both strong and weak frustration of the SQUID. In the regime of strong frustration $f \approx 0.5 \bmod 1$, the Josephson energies of the SQUID and the junction are almost equal. Under assumption of equal effective junction capacitances, this leads to comparable critical voltages $V_{c1} \approx V_{c2}$, with Bloch oscillations of similar strength. Because of the large coupling capacitance C_c, the synchronization of the Bloch oscillations has a substantial contribution to the overall voltage drop with $V_+ \approx V_{ci}$, see the Supplemental Material [25]. At weak frustration $f \approx 0 \bmod 1$, the SQUID arm becomes almost superconducting, see Fig. 3(b), with a large Bloch capacitance $C_B \gg C_c$, shunting the SQUID. As a result, it exhibits only weak Bloch oscillations effects with $V_{c2} \approx V_+ \approx 0$.

Figure 4(c) shows the regime of strong magnetic frustration corresponding to symmetric Josephson energies. The simulations show a synchronization of Bloch oscillations leading to a current mirror effect $I_{JJ} = -I_{SQ}$, whereas the synchronization leading to aligned currents is suppressed by thermal effects [25]. Figure 4(d) shows the regime of weak magnetic frustration corresponding to Bloch oscillations only in the single junction. The simulation points to the absence of synchronization, in this case, as well as a diminished blockade threshold also shown in Fig. 3(d).

Because of the strong junction-to-SQUID coupling $C_c > C$, the current I_{JJ} exhibits plateaus at the level scaling with the current $-I_{SQ}$ in the SQUID, as shown in Fig. 5(b). These plateaus emphasize the current mirror effect based on synchronization of Bloch oscillations. The synchronization can also be explicitly tracked in the time domain for the voltage drops $U_1(t)$ and $U_2(t)$ across the junction and SQUID, respectively. Figure 6(a) shows simulation results without noise, resolving oscillations on the scale of the inverse characteristic frequency. They indicate anticorrelated (or dipole-type) Cooper pair transfer in the two junctions, thus manifesting a current mirror effect on the microscopic scale. We note that the oscillation frequencies are matched even for asymmetric bias voltages, resulting in a small oscillating output current $I_{out} = I_{JJ} + I_{SQ}$, with an average close to zero, as shown in Fig. 6(b).

The simulations exhibit good agreement with the experimental data for small bias currents, $I_{JJ,SQ} \lesssim 0.5$ nA $\ll \pi e E_J^2/4\hbar E_C \approx 16$ nA, with negligible rate of Landau-Zener tunneling (see, e.g., Ref. [26]). At higher currents, the Bloch oscillation effects vanish behind the inelastic Cooper pair transport, which shows up as softening of the "backbending" in the measured I-V curves in

Figs. 3(b) and 5(a) as compared to Figs. 3(d) and 5(b), respectively.

To conclude, we have shown synchronization of coherent Bloch oscillations in a coupled circuit with ultrasmall Josephson junctions. In particular, we observed a current mirror effect and related plateaus of constant current in the dc I-V curves of the junctions. We have supported our interpretation of the data by theoretical analysis showing good qualitative agreement in a sub-GHz range, where the synchronization effect is pronounced. The demonstrated current plateaus are akin to the first dual Shapiro step, which paves the way toward the development of a quantum current standard. In the future, it would be interesting to optimize the current plateaus. In particular, the numerical simulations indicate that increasing C_c will further stabilize the synchronization and thus the current mirror effect.

Fruitful discussions with A. Zorin and L. Grünhaupt are appreciated. The authors acknowledge technical support from P. Hinze and T. Weimann. This work was supported by the Deutsche Forschungsgemeinschaft (DFG) under Grants No. HA 7084/6–1 and No. LO 870/2–1.

*Sergey.Lotkhov@ptb.de

[1] E. O. Göbel and U. Siegner, *The New International System of Units (SI): Quantum Metrology and Quantum Standards*, (Wiley-VCH, New York, 2019).
[2] B. Jeanneret and S. P. Benz, Application of the Josephson effect in electrical metrology, Eur. Phys. J. Spec. Top. **172**, 181 (2009).
[3] S. P. Giblin, G. Yamahata, A. Fujiwara, and M. Kataoka, Precision measurement of an electron pump at 2 GHz; the frontier of small dc current metrology, Metrologia **60**, 055001 (2023), and the references therein.
[4] K. K. Likharev and A. B. Zorin, Theory of the Bloch-wave oscillations in small Josephson junctions, J. Low Temp. Phys. **59**, 347 (1985).
[5] L. Kuzmin, Yu. Pashkin, A. Zorin, and T. Claeson, Linewidth of Bloch oscillations in small Josephson junctions, Physica (Amsterdam) **203B**, 376 (1994).
[6] R. S. Shaikhaidarov, K. H. Kim, J. W. Dunstan, I. V. Antonov, S. Linzen, M. Ziegler, D. S. Golubev, V. N. Antonov, E. V. Il'ichev, and O. V. Astafiev, Quantized current steps due to the a.c. coherent quantum phase-slip effect, Nature (London) **608**, 45 (2022).
[7] N. Crescini, S. Cailleaux, W. Cuichard, C. Naud, O. Buisson, K. Murch, and N. Roch, Evidence of dual Shapiro steps in a Josephson junction array, Nat. Phys. **19**, 851 (2023).
[8] J. E. Mooij and Yu. V. Nazarov, Superconducting nanowires as quantum phase-slip junctions, Nat. Phys. **2**, 169 (2006).
[9] S. Corlevi, W. Guichard, F. W. J. Hekking, and D. B. Haviland, Phase-charge duality of a Josephson junction in a fluctuating electromagnetic environment, Phys. Rev. Lett. **97**, 096802 (2006).
[10] F. Maibaum, S. V. Lotkhov, and A. B. Zorin, Towards the observation of phase-locked Bloch oscillations in arrays of small Josephson junctions, Phys. Rev. B **84**, 174514 (2011).
[11] L. Arndt, A. Roy, and F. Hassler, Dual Shapiro steps of a phase-slip junction in the presence of a parasitic capacitance, Phys. Rev. B **98**, 014525 (2018).
[12] A. Kitaev, Protected qubit based on a superconducting current mirror, arXiv:cond-mat/0609441.
[13] H. Shimada and P. Delsing, Current mirror effect and correlated Cooper-pair transport in coupled arrays of small Josephson junctions, Phys. Rev. Lett. **85**, 3253 (2000).
[14] F. Lecocq, I. M. Pop, Z. Peng, I. Matei, T. Crozes, T. Fournier, C. Naud, W. Guichard, and O. Buisson, Junction fabrication by shadow evaporation without a suspended bridge, Nanotechnology **22**, 315302 (2011).
[15] G. J. Dolan, Offset masks for lift-off photoprocessing, Appl. Phys. Lett. **31**, 337 (1977).
[16] F. Kaap and S. Lotkhov, High-kinetic-inductance microstrip wiring and a frequency-related Cooper pair current in ultrasmall Josephson junctions, Proc. Conf. Precis. Electromagn. Meas. **77**, 165 (2022).
[17] L. Grünhaupt, Granular aluminium superinductors, Ph.D. Thesis, 2019.
[18] P. Kamenov, W.-S. Lu, K. Kalashnikov, T. DiNapoli, M. T. Bell, and M. E. Gershenson, Granular aluminum meandered superinductors for quantum circuits, Phys. Rev. Appl. **13**, 054051 (2020).
[19] H. Rotzinger, S. T. Skacel, M. Pfirrmann, J. N. Voss, J. Münzberg, S. Probst, P. Bushev, M. P. Weides, A. V. Ustinov, and J. E. Mooij, Aluminium-oxide wires for superconducting high kinetic inductance circuits, Supercond. Sci. Technol. **30**, 025002 (2017).
[20] S. Lotkhov, Ultra-high-Ohmic microstripline resistors for Coulomb blockade devices, Nanotechnology **24**, 235201 (2013).
[21] A. B. Zorin, The Thermocoax cable as the microwave frequency filter for single electron circuits, Rev. Sci. Instrum. **66**, 4296 (1995).
[22] M. Büttiker, Zero-current persistent potential drop across small-capacitance Josephson junctions, Phys. Rev. B **36**, 3548 (1987).
[23] Our simulations show that for Bloch currents below $e\omega_p/\pi \sim 0.4$ nA, a lumped-element, purely capacitive approximation neglecting kinetic inductance term appears to be qualitatively adequate.
[24] Our estimations point to an intensive electron overheating in the titanium resistors, e.g., $T_{\mathrm{eff}} \sim 150$ mK at the bias current 100 pA [20]. Stronger oxidized titanium and thicker films can be helpful to reduce this effect in the future.
[25] See Supplemental Material at http://link.aps.org/supplemental/10.1103/PhysRevLett.132.027001 for a detailed discussion of this model.
[26] U. Geigenmüller and G. Schön, Single electron effects and Bloch oscillations in normal and superconducting tunnel junctions, Physica (Amsterdam) **152B**, 186 (1988).